# Isotopic molybdenum total neutron cross section in the unresolved resonance region

R. Bahran,[1,*] D. Barry,[2] R. Block,[2] G. Leinweber,[2] M. Rapp,[2] A. Daskalakis,[1] E. Blain,[1] D. Williams,[1,†] B. McDermott,[1] L. Leal,[3] and Y. Danon[1]

[1]*Gaerttner LINAC Center, Rensselaer Polytechnic Institute, Troy, New York 12180, USA*

[2]*Bechtel Marine Propulsion Corp., Knolls Atomic Power Laboratory, P.O. Box 1072, Schenectady, New York 12301, USA*

[3]*Oak Ridge National Laboratory, Oak Ridge, Tennessee 37831-6171, USA*

(Received 20 November 2014; published 4 August 2015)

Accurate isotopic molybdenum nuclear data are important because molybdenum can exist in nuclear reactor components including fuel, cladding, or as a high yield fission product. High-resolution time-of-flight neutron transmission measurements on highly enriched isotopic metallic samples of $^{95}$Mo, $^{96}$Mo, $^{98}$Mo, and $^{100}$Mo were performed in the resonance energy range from 1 to 620 keV. The measurements were taken with the newly developed modular $^{6}$Li-glass transmission detector positioned at the 100-m experimental flight station. In the unresolved energy region (URR), new comprehensive methods of analysis were developed and validated in order to obtain accurate neutron total cross-section data from the measurement by correcting for background and transmission enhancement effects. Average parameters and fits to the total cross section for $^{95}$Mo were obtained using the Hauser-Feshbach statistical model code FITACS, which is currently incorporated into the SAMMY code. The fits to the experimental data deviate from the current evaluated nuclear data file/B-VII.1 isotopic Mo evaluations by several percent in the URR.

DOI: 10.1103/PhysRevC.92.024601 PACS number(s): 25.40.−h, 28.20.−v

## I. INTRODUCTION

High accuracy nuclear data are important in their application to neutron transport calculations used in the design and analysis of reactor fuel cycles, fusion systems, astrophysical systems, nuclear nonproliferation, safeguards, criticality safety, stockpile stewardship, radiation protection, shielding calculations, particle physics, and medical physics research. Experimental high accuracy data also help contribute to the growing understanding of nuclear reaction theory. In the unresolved resonance region (URR), an accurate representation of the shape of the cross section can help validate nuclear models developed to understand the underlying physical processes of nuclear reactions and to predict general cross-section behavior. This paper reports neutron time-of-flight (TOF) transmission measurements of highly enriched metallic samples of $^{95}$Mo, $^{96}$Mo, $^{98}$Mo, and $^{100}$Mo that were performed at the Gaerttner LINAC Center at Rensselaer Polytechnic Institute (RPI) in the energy range from 1 to 620 keV. It also describes a new evaluation of a $^{95}$Mo total cross section in the unresolved resonance range. Isotopic molybdenum total neutron cross-section data in particular are important because molybdenum can exist in nuclear reactors as a high yield fission product or in alloyed form with applications in reactor piping, fuel cladding, and most importantly in advanced nuclear fuel in the form of U-Mo [1–3]. U-Mo alloys are mechanically stable, possess high thermal conductivity, are corrosion resistant in a high-temperature water environment (more so than unalloyed uranium), and are highly durable under high levels of irradiation [2–4]. They also are characterized by a high density of uranium, leading low enriched uranium-Mo alloy fuel to become the designated replacement fuel for research reactors currently operating with highly enriched uranium while still being able to achieve high neutron fluxes [2–4]. Molybdenum is also in the makeup of many important fast burst criticality benchmarks. Recently, U-Mo has also been highlighted as a viable fuel candidate for small fission space power reactors [3]. A comprehensive overview of the physical, thermal, mechanical properties, and fuel performance topics for U-Mo alloys can be found in Refs. [2–4].

## II. ISOTOPIC MOLYBDENUM CROSS-SECTION EVALUATION

### A. Resolved resonance region

The observed resonance structure in neutron cross sections is a result of the discrete energy levels of the compound nucleus where isolated resonances are characterized by what are known as resolved resonance parameters. At some point in energy, only the partially resolved structure is observed as the experimental resolution becomes comparable to the average natural width of the resonances. These unresolved multiples of resonances can also exist due to the level spacing between isolated resonances becoming comparable to their average natural width. This transitional region is often referred to as the unresolved resonance region. For molybdenum, previous isotopic measurements have provided cross-section libraries of resolved resonance parameters up to 2.1 keV for $^{95}$Mo, 19.5 keV for $^{96}$Mo, 52.6 keV for $^{98}$Mo, and 26.1 keV for $^{100}$Mo [5,6]. New high-resolution isotopic molybdenum total cross-section data were measured at RPI and include newly resolved resonances allowing an extension of the resolved resonance region. For $^{95}$Mo, new resonance parameters between $E_n$ = 5–20 keV were determined for 180 newly resolved resonances

*Present address: Los Alamos National Laboratory, Los Alamos, New Mexico 87545; bahran@lanl.gov

†Present address: United States Military Academy, West Point, New York 10966.

 

that were fitted from the experimental data [7] using the *R*-matrix code SAMMY [8]. For the $^{95}$Mo measurement and evaluation in the resolved resonance region, the biggest limitation is caused by finite-energy resolution, which leads to missing level contributions in the unresolved region. These missing contributions were evident in two empirical metrics as compared to previously reported values. A calculated value of the neutron strength function based on an analysis of the experimental data which extends the resonance region up to 50 keV was lower than values reported in the *Atlas of Neutron Resonances* [5,7]. There was also a divergence from theoretical estimates based on previous values in the plotted cumulative levels [7]. At higher energies, the contributions of the missing levels become more important, and an unresolved resonance treatment of the experimental data could prove to be more useful. Therefore, based on observations of the cumulative levels from the analysis of the new dataset, it can be concluded that the evaluated nuclear data file (ENDF)/B-VII.1 upper energy boundary of 2.2 keV for $^{95}$Mo is reasonable [7]. This choice of an upper energy boundary for the resolved resonance region is ultimately decided upon by nuclear data evaluators who can determine the performance of different data treatments on major experimental benchmarks. The upper resolved resonance region boundary can differ significantly between evaluated libraries depending on the differential data and integral benchmark used in the evaluation. For example, evaluators in Japan scaled back the upper resolved resonance region boundary for $^{235}$U from 2.25 keV (current ENDF/B-VII.1 value) to 500 eV for JENDL-4.0 [9].

### B. Unresolved resonance region

In the unresolved resonance region, the underlying structure that leads to the observed partially resolved structure still needs to be characterized. This is especially important for use in neutron transport calculations in codes, such as MCNP [10] or OPENMC [11] in order to account for resonance self-shielding effects. Average resonance parameters extracted from experimental data are used to produce probability distribution functions representing the total neutron cross section (whose mean value is the infinitely dilute smooth average of the cross section) at discretized energies [12]. These distribution functions are represented in tabular form for application in Monte Carlo codes and are referred to as "probability tables" [12]. For MCNP or OPENMC, which have many applications and are used worldwide, the cross-section processing code NJOY [13] can generate probability tables from a "ladder" of sampled resonances based on average parameters and statistical laws (Wigner spacing for resonance energies, single level Breit-Wigner for resonance shapes, Porter-Thomas $\chi^2$ distributions for resonance widths, and $\psi-\chi$ Doppler broadening) [12,14]. Average parameters based on new experimental data provide a more reliable sampling distribution for these ladders. This will ultimately allow higher accuracy Monte Carlo calculations, which may be used to improve neutronics calculations and better quantify safety margins in nuclear reactor designs.

The goal of the present analysis was to obtain new fits and extract average resonance parameters in the unresolved resonance region from the new total cross-section measurements in an ENDF-compatible format. In this format, URR cross sections are computed from average resonance parameters in ENDF file 2 and the dilute cross section in file 3 [15]. It is generally expected that the infinitely dilute cross section in file 3 should be obtained from the best combination of measurements and models as provided by evaluators [16]. The average resonance parameters are used to determine the energy self-shielding of the cross section, which is very important for reactor calculations. Furthermore, it has been proposed, that the unsmoothed high-resolution total cross-section experimental data in this region should be stored directly [17,18] in evaluated files to be available to users (who typically plot the infinitely dilute cross section versus energy without any self-shielding [14]). How these files are used is determined by an ENDF-102 "LSSF" flag. This flag indicates (when equal to 1) that the file 2 average resonance parameters contained in probability tables are converted to self-shielding factors and then multiplied by the cross section in file 3 [14].

The $^{95}$Mo total cross-section upper boundary for average parameters in the unresolved region extends to 206 keV for ENDF/B-VII.1 and JEFF-3.1.2 and 400 keV for JENDL-4.0. In this present paper, new average parameters and fits to the total cross sections were obtained for $^{95}$Mo between $E_n$ = 190–590 keV. The starting point of the analysis was chosen near the cutoff of the current upper boundary of the ENDF/B-VII.0 library. The fits and average parameters were obtained from the measurement using the Bayesian Hauser-Feshbach statistical model code FITACS [19], which is currently incorporated into the SAMMY Bayesian analysis code [8]. These parameters can improve the existing library database by better representing the structure in the URR. The new results have been made available in a format that is compatible with ENDF extending the region where average parameters are available in ENDF to 590 keV [7]. The final upper boundary for average parameters should still be determined by evaluators and users at an energy where self-shielding and temperature-broadening applications become negligible [15].

## III. EXPERIMENTAL SETUP

The high-resolution transmission measurements were taken with the newly developed Mid-Energy $^6$Li-glass Neutron Detector Array (MELINDA) [20] positioned at the 100-m experimental flight station. MELINDA employs four identical cubic modules each with a 0.5-in.-thick $^6$Li-glass scintillator, two 5-in. diameter out-of-beam photomultiplier tubes coupled to fast-timing electronics, and a low-mass light-tight aluminum casing with inner mirrorlike reflective surfaces. The dead time of the system was set to be 430 ns requiring corrections no larger than 5%.

A detailed computer-aided design model of MELINDA is shown in Fig. 1. The modular design of the detector array allows operational reliability, relatively easy maintainability, and lower overall life-cycle costs than a single all-in-one detector system. It also provides functional versatility. For example, different detector module placements can provide a neutron-scattering detector or an in-beam neutron monitor.

Flight tubes are positioned between the detector and the photoneutron target, providing an evacuated pathway for the

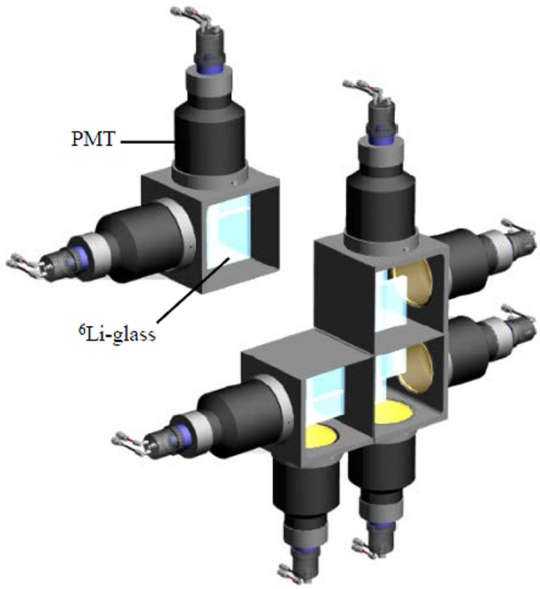


FIG. 1. (Color online) Detailed three-dimensional computer model of the midenergy $^{6}$Li-glass neutron detector array.

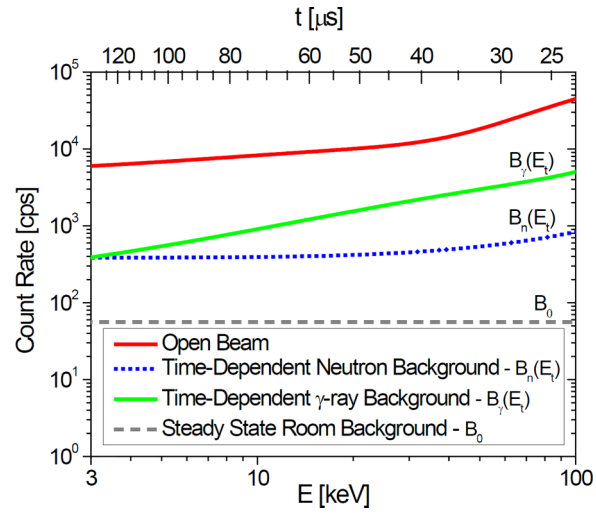


FIG. 2. (Color online) Decomposition of the background shapes observed by the $^{6}$Li-glass detector during measurements.

neutrons to travel. Neutrons are generated at the Gaerttner LINAC when short bursts of energetic electrons (≈50 MeV) are directed at a water-cooled and water-moderated tantalum target [21]. A water-moderated photoneutron tantalum target [22] was used in the high-resolution transmission measurements utilizing a 12-ns electron burst width from the linear accelerator. The average current on target during the measurements was 22 $\mu$A.

The measurements were performed with a fixed $^{10}$B-enriched boron disk to minimize overlap neutrons between LINAC pulses. Additionally, a high-$Z$ filter was inserted in the beam (5/8-in. Pb or 1-in. $^{238}$U) to reduce the low-energy $\gamma$-ray background and initial high-energy $\gamma$-ray burst both generated by the target. A new method to measure the different background components (neutron and $\gamma$ ray) was performed by cycling different materials with strong black resonances into the beam. The dominant time-dependent $\gamma$-ray background component, which is mainly a result of thermal neutron capture in the target tantalum and water moderator, was determined by placing several thicknesses of polyethylene in the beam and extrapolating the $\gamma$-background to zero-thickness polyethylene as shown in Fig. 2. Black notch filters of Na, Al, Mg, S, Li, and Be were used to determine the time-dependent neutron background at specific energies across the energy range of interest.

Highly enriched (<95%) metallic samples of isotopic molybdenum were prepared by Oak Ridge National Laboratory for these measurements. The full isotopic compositions of the samples were provided by the manufacturer. The samples were mounted to aluminum disks that were placed onto a computer-controlled sample changer located at an ∼13-m flight distance from the neutron-producing target. The atomic composition and areal number density of the samples were known to high precision and are shown in Table I. The uncertainty in the number density includes the uncertainty from the enrichment.

## IV. DATA ANALYSIS METHOD

The data analysis method is a four-step process outlined below. It includes reducing the data to cross section, correcting for energy-averaged transmission enhancement, testing for intermediate structure, and obtaining total neutron cross-section fits and average parameters using SAMMY.

### A. Data reduction to cross section

The transmission of neutrons through the material is denoted as $T_i$ and is defined as the ratio of background corrected count rate in counts per second with the sample material in the beam to the background corrected rate in the open beam in TOF channel $i$,

$$T_i = \frac{\left[C_i^{\text{sample}} - B_i^{\text{sample (steady state)}} - B_i^{\text{sample}}\right]}{\left[C_i^{\text{open}} - B_i^{\text{open (steady state)}} - B_i^{\text{open}}\right]}, \qquad (1)$$

where $C_i^{\text{sample or open}}$ is the dead-time corrected and monitor-normalized count rate of the sample or open measurement, $B_i^{\text{sample or open (steady state)}}$ is the steady-state background counting rate for the sample or open measurements, and $B_i^{\text{sample or open}}$ is the time-dependent background count rate [1]. Transmission data reduction was performed using the internal processing codes RPIXDR, MONCHK, BACK, FIT, and

TABLE I. Sample enrichment and number density.

| Isotope | Enrichment % | Atoms/barn of isotope |
|---|---|---|
| $^{95}$Mo | 96.5 ± 0.1 | 0.03857 ± 0.00007 |
| $^{96}$Mo | 96.8 ± 0.1 | 0.05470 ± 0.0001 |
| $^{98}$Mo | 95.83 ± 0.03 | 0.03687 ± 0.00004 |
| $^{100}$Mo | 95.36 ± 0.24 | 0.05188 ± 0.0002 |

TRANS. RPIXDR produces dead-time-corrected, run-summed, and monitor-normalized data files that can be grouped and displayed in counts per second. Statistical checks and correlations between beam monitor data and time-of-flight transmission data were performed with MONCHK. For background corrections, a function was fitted through the experimentally determined background points and subtracted from the data. The experimental transmission and its associated error were determined by TRANS. The total cross section is related to the transmission by

$$T(E) = \exp\left[-N\sigma_t(E)\right], \tag{2}$$

where $N$ is the areal number density of the sample in atoms/barn, $T(E)$ is the probability of a neutron of energy $E$ to pass through the sample without interaction, i.e., the transmission, and $\sigma_t$ is the total microscopic neutron cross section. When converting the experimental data to transmission, all of the isotopes in the highly enriched samples were accounted for.

Direct comparisons to previous isotopic measurements in the URR with broader resolution or elemental measurements with comparable resolution [23] are difficult. The ability to observe resonance structure in the unresolved region depends on the level density of the isotopes (affected by the purity of the sample), sample thickness, statistical accuracy of the measurement, and the maximum energy resolution of the experiment. A detailed characterization of the resolution of the experimental apparatus is available in Ref. [7]. To illustrate this type of structure, the final cross-section data for $^{100}$Mo were compared to four reference experimental datasets [24–26] on which the latest ENDF/B-VII.1 total cross section is based in this energy range [6]. A portion of the present high-resolution data as compared to previous data and the latest evaluation is shown in Fig. 3. A partially resolved structure can be clearly observed in the new measurement of $^{100}$Mo (a similar structure is observed in $^{96}$Mo and $^{98}$Mo). The goal of this analysis is to represent the underlying structure in a format that is compatible with ENDF.

### B. Transmission enhancement correction

In transmission data, the presence of unresolved resonance structure can lead to an effective measured cross section that is lower than the true average cross section. This enhancement of the energy-averaged transmission [18] results when the energy-averaged bins of the measured data are larger than the widths of the underlying structure. This can be a result of manually averaging the transmission, resolution energy broadening, or transitioning into the region where the level spacing between resonances becomes comparable to the average natural widths. This phenomenon is best described by considering the mathematical relationship between the true average cross section and the average transmission [27],

$$\langle\sigma_t\rangle = \frac{1}{N}\ln\langle e^{-N\sigma_t}\rangle + \frac{1}{N}\ln\left(1 + \frac{N^2}{2}\mathrm{var}\sigma_t - \ldots\right). \tag{3}$$

The first term is what is often incorrectly reported by measurers of high-resolution data as the experimental total cross section [18,27]. The subsequent terms, often neglected in theory, represent a correction containing the cross-section variance within the range of the resolution function and higher moments of its distribution quantifying the contribution of underlying resonances to the average cross section [18,27]. As Eq. (3) shows, the correction is large when the variance in the cross section is large and with thicker samples, i.e., larger $N$, as illustrated in Fig. 4. The higher-resolution data require a smaller transmission enhancement correction, i.e., when high-resolution cross-section data are averaged over smaller energy bins and thus over fewer fluctuations, it provides values that are closer to the theoretical average. If the resonances in a transmission dataset are fully resolved, then the correction approaches unity.

The most accurate correction can be calculated directly with transmission data from two different sample thicknesses using a rigorous method developed by Fröhner and Larson that used the data directly by solving a pair of equations derived from Eq. (3) [18]. This method was previously implemented using elemental molybdenum transmission data

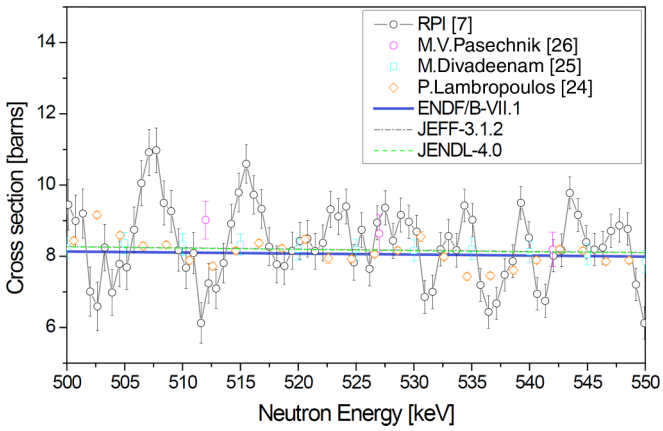


FIG. 3. (Color online) New $^{100}$Mo experimental data compared to previous data upon which the current major evaluations (ENDF, JEFF, and JENDL) are based.

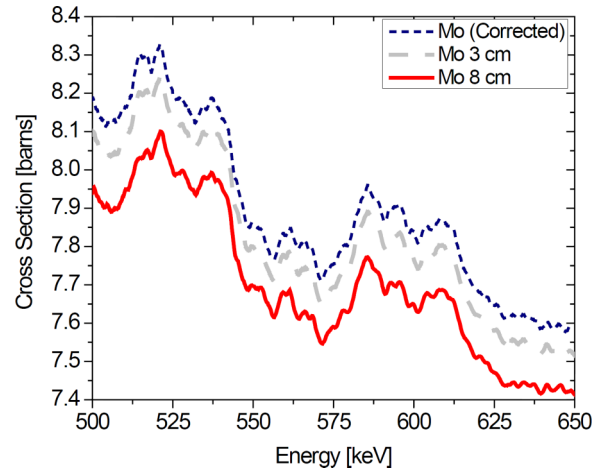


FIG. 4. (Color online) Example of the Fröhner and Larson correction [18] on elemental molybdenum transmission data with a thick sample.

obtained from two comparatively thick samples of 3 and 8 cm (0.189 29 and 0.5114 atoms/barn, respectively) measured at the 100-m experimental flight station [23]. The calculated average correction based on the method of Fröhner and Larson for the 3-cm sample was 0.7% between 500 and 650 keV as shown in Fig. 4. For the isotopic Mo experiments, only one sample thickness for each isotope was measured. Thus, determining the transmission enhancement correction could only be quantified based on information obtained from the resolved resonance region. Several methods were evaluated in order to determine the transmission enhancement correction based on average resolved resonance parameters using the codes SAMMY, MCNP5, and SESH [28] as described below.

#### 1. Correction with SAMMY

SAMMY was previously used by Derrien *et al.* [29] to provide this correction to keV-energy transmission data of $^{238}$U by shifting resonance parameters from the resolved resonance region to higher energies to obtain a computational estimate of the true average cross section using SAMMY. The level spacing was not changed, but the reduced neutron widths were multiplied by $\sqrt{E_0/E_{\text{shifted}}}$ when shifted to higher energies. The estimate of the true average cross section, which can also be obtained with Monte Carlo sampling, was then compared to the effective average also obtained using SAMMY. The effective average was obtained by Doppler broadening the estimate of the true average cross section converting this value of $\sigma_t^D$ to transmission using Eq. (2) and averaging over the resolution $R(E)$ [29],

$$T(E) = \int \exp\left[-N\sigma_t^D(E)\right] R(E - E')dE', \qquad (4)$$

and then converting back to the cross section. The energy-dependent resolution function can be determined experimentally by measuring well-known resonances in the resolved resonance region or with Monte Carlo simulations of the experimental setup. Its average effect can also be estimated by varying the resolution in the simulated data until the standard point-to-point deviation matched that of the experimental data. This method worked well for $^{238}$U, which has many resonances in short energy intervals providing an adequate statistical sample when "copying" resonances. When performed on $^{95}$Mo, this method failed to show agreement with the energy-dependent correction shape obtained with other methods. Furthermore, uncertainties associated with the SAMMY method are difficult to quantify and can arise from the incorporation of the experimental resolution, inaccurate representation of the level spacing, width, strength, averaging methodology, and energy bin width selected for the calculation.

#### 2. Correction with MCNP

Alternatively, a method based on Monte Carlo sampling of ladders has been adopted by other researchers [18,30]. Such a correction must only be applied to cross sections obtained from smoothed transmission data. One way of determining this correction was by simulating a transmission experiment of the measured sample in MCNP. The correction was obtained by comparing the resulting transmissions when the probability tables in MCNP were turned on and off. This method can be applied only to energies where probability tables for the unresolved resonance region are available in the processed library data used by MCNP. For $^{95}$Mo this end point was at 206 keV. This limitation can be mitigated by using NJOY in order to extend this upper boundary and include resonance parameters experimentally obtained from analysis of the samples of interest.

#### 3. Correction with SESH

For the present paper, the energy-dependent correction based on the SESH code [28] was adopted for the measured isotopic molybdenum samples. SESH can calculate corrections for simple geometry samples of up to ten medium or heavy weight nuclei between 5 and 500 keV based on Monte Carlo sampling of known average parameters [28]. SESH includes contributions from $s$-, $p$-, $d$-, and $f$-wave levels [28] with the condition that the experimental transmission does not contain significant structure; otherwise, additional smoothing is required. The initial SESH input parameters for all of the isotopes in the sample were obtained from the ENDF/-VII.1 library [6] and the *Atlas of Neutron Resonances* [5]. These parameters included the sample thickness, isotopic abundance, ratio of nuclear mass to neutron mass, binding energy, pairing energy, effective temperature, scattering radius, strength functions, average level spacing, and average radiative width. The initial SESH correction is shown in Fig. 5 and was compared to example results obtained using the MCNP5. MCNP5 provided correction values that are slightly larger than SESH values, consistent with results reported by Noguere [31]. After the initial correction was applied to the cross section obtained from smoothed experimental transmission between $E_n$ = 190–590 keV (averaged in TOF), new strength functions from the SAMMY analysis based on the corrected data were used to obtain an updated SESH correction factor in the same energy range. The updated SESH correction factors were then used to correct the initial data again, thus making this process iterative. The SESH correction values converged after three

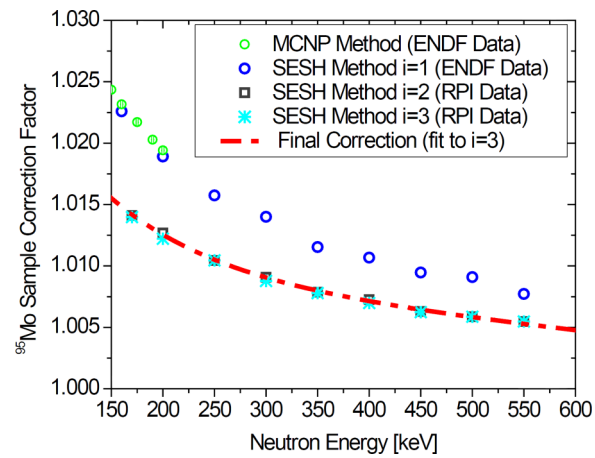


FIG. 5. (Color online) Exponential fit to the final $^{95}$Mo transmission enhancement correction obtained from different SESH iterations ($i$ = 1–3).

iterations as shown in Fig. 5. The final SESH correction that was applied to the data was <1.4%, which was on par with the average statistical uncertainty ($1\sigma$) in the experimental total cross section in this region (1.5%). The uncertainty on the correction was neglected in the present paper.

### C. Testing for intermediate structure

Nonstatistical fluctuations in the observed experimental cross section in the unresolved region indicated the existence of either partially resolved overlapping compound nucleus resonance structure or intermediate structure [32]. Intermediate structure is characterized by an intermediate width that is much larger than the width and spacing of the compound nuclear levels but smaller than the structure and spacing of the optical model shaped resonances [33]. Such a structure has been described by Feshbach *et al.* [33] and others in terms of "doorway states," a simple mode of excitation whose complexity falls in between the optical model single-particle states and the compound nuclear states [33].

Intermediate structure cannot be represented by average parameters obtained from FITACS that are based on the conventional Hauser-Feshbach model. Therefore, a widely used method [24,34] was applied to determine the existence of intermediate structure based on the interferential fluctuations in the experimental data. Other methods [24,35,36] have also been described. In his seminal paper [34], Pappalardo proposes an autocorrelation function $C(\Delta)$ to test for the presence of intermediate structure in the energy-dependent total cross section $\sigma(E)$ [24,34],

$$C(\Delta) = \frac{1}{N}\sum_{i=1}^{N}[\sigma(E_i) - \overline{\sigma(E_i)}]^2, \tag{5}$$

where

$$\overline{\sigma(E_i)} = \frac{1}{\Delta}\int_{E_i-0.5\Delta}^{E_i+0.5\Delta}\sigma(E)dE, \tag{6}$$

and $\Delta$ is the averaging interval. This autocorrelation function was evaluated using the experimental cross section for each isotopic measurement over the energy range of 200–500 keV for $^{95}$Mo and plotted as a function of the averaging interval as shown in Fig. 6. As $\Delta$ approaches the width of the fluctuations due to statistics or fluctuations due to the partially resolved compound nucleus structure, $C(\Delta)$ rises with the increasing in $\Delta$ [34]. As $\Delta$ surpasses the width of the these fluctuations, $C(\Delta)$ should approach a constant value if intermediate structure is absent [34]. Another rise would indicate the existence of an additional intermediate width in this region (expected to be on the order of 10–100 keV) [24]. Although some variation can be observed, no substantial second rise was apparent in the dataset shown in Fig. 6 indicating only a partially resolved compound nucleus structure.

### D. URR analysis in SAMMY

Fits to the neutron total cross section were obtained using the Hauser-Feshbach (with width fluctuations) statistical model code FITACS [19], which is incorporated into the SAMMY code [8]. This option has the features of providing comprehensive treatment of the data, immediate availability, and ability to produce average resonance parameters and cross-section datasets with covariances in files compatible with ENDF. Average parameters were obtained by fitting the calculated theoretical cross section to the experimental isotopic Mo cross-section dataset by solving the Bayes' equation relative to several variable parameters. The average parameters included the neutron strength functions for $s$-wave, $p$-wave, and $d$-wave resonances, the average level spacing $D$, and the "effective" or "potential scattering radius" [15] $R'$. In SAMMY, the energy dependence was obtained from the giant dipole model for the capture widths, the Bethe formula for the mean level spacing for $l > 0$, and the Gilbert-Cameron composite formula for $s$-wave mean level spacing [8,18]. The starting values of the input parameters typically should not diverge outside of the constraints of the theory in order to obtain realistic results. Initial values were mainly adopted from the *Atlas of Neutron Resonances* [5] based on a statistical analysis of the resolved resonance region. The neutron strength functions for $s$-wave, $p$-wave, and $d$-wave resonances ($l = 0$–2) were adopted directly from the *Atlas of Neutron Resonances* [5]. The strength functions for $s$-wave and $p$-wave resonances were both varied during the fitting procedure. The average radiative capture width parameters and level spacing for $s$-wave and $p$-wave resonances were also obtained from the atlas [5]. The initial $d$-wave parameters were adopted as the same value as the $s$-wave parameters since both are expected to have a small contribution in this region (a method to obtain an estimate of values for $l > 1$ can be found in Ref. [37]). The initial value of the varied $s$-wave distant-level parameter $R^{\infty}$ was obtained from its relationship to the effective or potential scattering radius [15] $R'$ adopted from the atlas [5] and the channel radius $a$ [38],

$$R_l^{\infty} = 1 - R'/a, \tag{7}$$

where $a$ is the channel radius ("hard-sphere radius" or nuclear radius [15]) with units of Fermi [29],

$$a = 1.23([A/m_n]^{1/3} + 0.8), \tag{8}$$

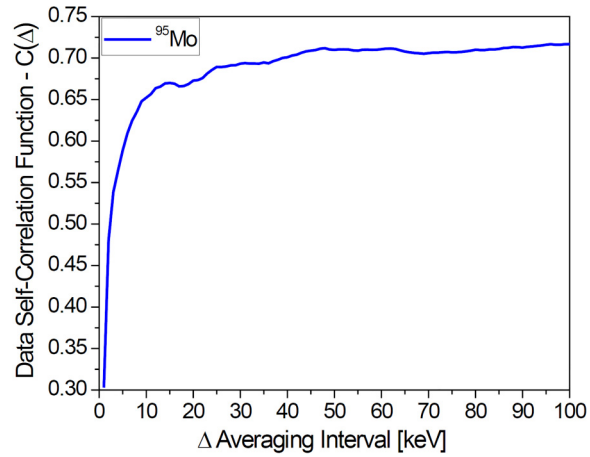


FIG. 6. (Color online) Test for intermediate structure in the $^{95}$Mo experimental cross-section data based on the Pappalardo autocorrelation function [34].

where $A$ is the atomic weight of the sample isotope and $m_n$ is the mass of the neutron both in atomic mass units. The distant-level parameter $R^{\infty}$ is energy dependent and represents the contributions from resonances above and below a given energy [38]. Varying the distant-level parameter varies the scattering radius $R'$ since the channel radius must remain constant (there is no theoretical justification to vary the channel radius [38]). Additional input parameters are required that cannot be varied. Such parameters include the binding energy or "neutron separation energy" $S_n$, which was obtained from the atlas [5] which reports values based on Ref. [39]. The neutron pairing energy is zero for $^{95}$Mo (odd $A$) and $+a_p A^{-3/4}$ for the other even-even Mo isotopes where $a_p = 34$ MeV and is an empirically based constant [40]. The energies of the nuclear excited states (inelastic states) were obtained from the National Nuclear Data Center evaluated nuclear structure data file [6]. SAMMY does not have the capability for URR analysis of multiple nuclides in one sample [8], so only the parameters for the enriched isotope were adopted. Due to the highly enriched nature of the samples, the effects of this limitation were determined to be negligible.

## V. RESULTS

### A. cross-section comparison to latest evaluation

Neutron total cross-section fits for $E_n = 175 - 590$ keV were obtained from SAMMY at a region where the transmission enhancement correction was on average approximately 1% (with a maximum value of approximately 2%). The final fits were evaluated by how well they reproduced the experimental cross section and how they compared to the latest total cross-section evaluated libraries as shown in Fig. 7. Error bars on the SAMMY fit are within the thickness of the line. The ENDF/B-VII.1, JEFF, and JENDL evaluations are nearly identical in the unresolved resonance region. The fits to the high-resolution experimental data deviate from the current isotopic $^{95}$Mo evaluations by up to 4% at some points in the unresolved resonance region. The cross sections in the URR

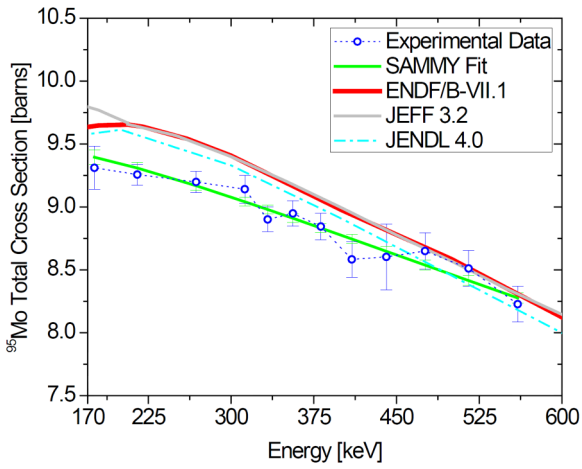


FIG. 7. (Color online) $^{95}$Mo SAMMY fit compared to data and evaluation. The fit to the new experimental data is slightly lower than the current evaluations across most of the graphed energy range.

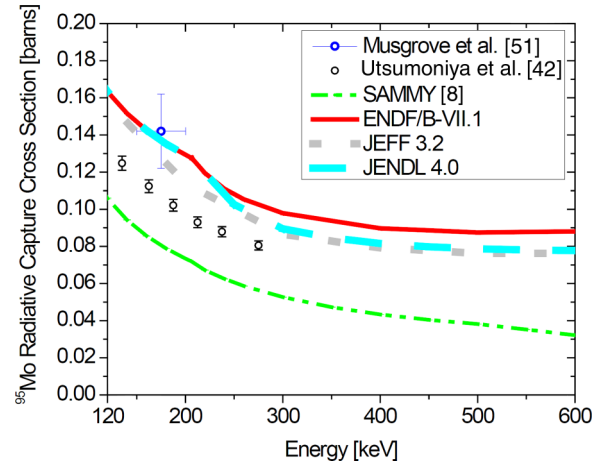


FIG. 8. (Color online) $^{95}$Mo theoretical capture cross-section results from the SAMMY analysis based on the total cross-section data compared to the latest ENDF evaluation. The experimental values plotted consist of those available in the EXFOR database and data measured by Koehler [41], which also appear in [42].

calculated by ENDF processing codes typically provide a less accurate representation of the actual cross section than those obtained from SAMMY as they do not use the same formulas [8].

The evaluated $^{95}$Mo capture cross section is <3% of the total measured cross section. Evaluated capture data were included in the FITACS analysis of the total cross section. The resulting theoretical capture cross-section output from FITACS was consistently lower than the current ENDF evaluation as shown in Fig. 8. It is also lower than the stand-alone experimental data point obtained from exchange format (EXFOR) (Musgrove *et al.* [51]. The FITACS values are in closer agreement with a recent analysis of data that was measured by Utsumoniya *et al.* at the Oak Ridge Electron Linear Accelerator [42].

Currently, capabilities are being developed at the Gaerttner LINAC Center that will allow complementary capture cross-section measurements in the keV region [43]. If new capture measurements are obtained, the overall fitting procedure in the URR using SAMMY can be performed sequentially where the results and covariances of one run file can be used as input for another dataset [8].

### B. Average parameters

The fitted quantities from SAMMY were the neutron strength functions $S_{l=0,1}$ and the potential scattering radius $R'$. The average radiative width $\Gamma_\gamma$ was not varied since it is well known from the resolved resonance region. Past elemental molybdenum transmission measurements at RPI reported the $s$-wave strength function for $^{95}$Mo that is in good agreement with the current evaluation [1]. The $s$-wave strength function is also expected to have a smaller contribution since at around $A = 90$–$100$ there is a minimum in the $s$-wave strength function and a peak (ten times stronger) in the $p$-wave strength function based on the optical model [5]. The strength function can be defined through its relationship to the average level

TABLE II. Comparison of isotopic $^{95}$Mo fitted quantities across the energy range of 100–620 keV. Quoted uncertainties are $1\sigma$ statistical uncertainties. The ENDF quantities are from the header blocks of the data files which do not quote uncertainties.

| | $^{95}$Mo | RPI | ENDF | Atlas |
|---|---|---|---|---|
| | $R'$ (fm) | $6.97 \pm 0.04$ | 7.00 | $7.00 \pm 0.2$ |
| | $10^4 S_0$ | $0.4 \pm 0.1$ | 0.45 | $0.47 \pm 0.17$ |
| $l = 0$ | $\Gamma_{\gamma 0}$(eV) | 0.150 | 0.150 | 0.160 |
| | $10^4 S_1$ | $3.8 \pm 0.1$ | 6.54 | $6.89 \pm 1.77$ |
| $l = 1$ | $\Gamma_{\gamma 1}$(eV) | 0.210 | 0.180 | 0.210 |

spacing and average reduced neutron width $\langle g\Gamma_n^l \rangle$ [5],

$$S_l = \frac{\langle g\Gamma_n^l \rangle}{(2l+1)D_l}. \quad (9)$$

Average resonance parameters and their covariances[1] were automatically extracted from the SAMMY fit for multiple energy groups and each quantum number and parity $J^\pi$. Ten energy groups were specified in this analysis providing average resonance parameters at intervals of ~40 keV. The results of the fits were compared to values from the resolved resonance region obtained from the newest edition of the *Atlas of Neutron Resonances* [5] and to the JENDL-4 library. ENDF/B-VII.1 only has average resonance parameters up to 206 keV. Therefore, comparisons were made to the latest JENDL-4 library instead of ENDF. These values can be used to determine energy-dependent self-shielding factors in Monte Carlo calculations based on the observed fluctuation in the cross section in each energy interval. The results were generally in agreement with previous evaluations, i.e., within $2\sigma$ of the experimental uncertainty of previous data as shown in Tables II and III. The *s*-wave neutron strength function was also consistent with values obtained from optical model calculations [5]. The only exception was the *p*-wave strength function, which was lower than reported values. This is attributed to the lower measured cross section. Since no capture dataset was used, the radiative width did not change. A snippet of the average parameters obtained is shown in Table III [7]. To facilitate evaluator review of the data for possible future incorporation into the major nuclear data libraries, the experimental data have been submitted to EXFOR. Full resonance parameters have also been obtained in evaluated form in ENDF-compatible format.

[1]The current ENDF format does not include a provision for including the uncertainty in the nuclear radius or energy-dependent uncertainty in the covariance representation of the average parameters in the URR.

TABLE III. Comparison of RPI $^{95}$Mo average resonance parameters to the JENDL evaluation which ends at 400 keV (ENDF ends at 206 keV).

| RPI $^{95}$Mo $S_{l=0}, J^\pi = +2.0$ | | | JENDL-4 $^{95}$Mo $S_{l=0}, J^\pi = +2.0$ | | |
|---|---|---|---|---|---|
| $E$ (keV) | $D$ (eV) | $g\Gamma_n^0$ (MeV) | $E$ (keV) | $D$ (eV) | $g\Gamma_n^0$ (MeV) |
| 196 | 155.29 | 0.0065 | 200 | 144.11 | 0.0080 |
| 237 | 149.87 | 0.0062 | | | |
| 279 | 144.66 | 0.0060 | 300 | 125.47 | 0.0070 |
| 320 | 139.63 | 0.0058 | | | |
| 362 | 134.79 | 0.0056 | | | |
| 403 | 130.12 | 0.0054 | 400 | 105.85 | 0.0059 |
| 445 | 125.62 | 0.0052 | | | |
| 486 | 103.50 | 0.0044 | | | |
| 528 | 99.89 | 0.0043 | | | |
| 569 | 96.42 | 0.0041 | | | |

## VI. CONCLUSIONS

New high-resolution total cross-section isotopic molybdenum measurements were performed for the stable molybdenum isotopes of $^{95,96,98,100}$Mo in the energy range between $E_n$ = 5–620 keV. In the unresolved region between $E_n$ = 190–590 keV, new average parameters and fits to the total cross sections for $^{95}$Mo were obtained. The upper boundary for average parameters in the unresolved region extends to 206 keV for ENDF/B-VII.1 and JEFF-3.1.2, 400 keV for JENDL-4.0, and 570 keV for the present paper. The final value should be determined by evaluators and users at an energy where self-shielding and temperature-broadening applications become negligible [15]. Below 190 keV, a large correction for the energy-averaged transmission was required for $^{95}$Mo. Measurements with two samples for these isotopes were not available to obtain a high accuracy correction. The new results have been made available in a format that is compatible with ENDF [7].

Results for the analysis of the $^{95}$Mo in the resolved resonance region are available in Ref. [7]. Data analysis of experimental data from other isotopically enriched samples ($^{92-94}$Mo, $^{96}$Mo, $^{98}$Mo, and $^{100}$Mo) are underway. The final molybdenum neutron total cross-section data and resonance parameters can help the international nuclear data user community and evaluators correct discrepancies between libraries and different theoretical models, e.g., experimental values of the neutron strength function can help refine optical model parameters where values are discrepant [5]. A recent intermediate benchmark paper shows that MCNP6 calculations with the latest major international libraries (ENDF/B-VII.1, JEFF-3.1.1, and JENDL-4.0) overestimate the measured results of an intermediate energy criticality experiment with molybdenum by 2% to 3% [43]. Additionally, several recent fast Mo integral benchmarks were compared to an MCNP5 model using the current ENDF/B-VII.1 evaluation and overestimated the measured results [44,45]. One of the fast benchmark sets were performed at the Russian Federal Nuclear Center utilizing a core of highly enriched uranium and two molybdenum end reflectors [44,46]. The other fast benchmark (average neutron energy ~200 keV) was performed in France at CEA-Valduc utilizing the fast-pulsed reactor CALIBAN, an unreflected highly enriched uranium metal core alloyed with 10 wt % molybdenum [46]. The results of the unresolved resonance region analysis for $^{95}$Mo support these benchmark conclusions since they lead to a total cross section that is lower than current

evaluated data by up to 4%. This difference is not accounted for in the absorption cross section and therefore is assumed to be scattering, which could reduce the reported intermediate and fast molybdenum benchmark discrepancy.

To fully quantify the impact of the new measurements, the data can be incorporated into Monte Carlo radiation transport models of integral criticality experimental benchmarks that include molybdenum. The models can incorporate data from the present paper that can be combined with complementary data of isotopic molybdenum measured at the Gaerttner LINAC Center at Rensselaer. This includes high-resolution molybdenum total cross-section data for the energy range between 0.5 and 20 MeV that were measured at a 250-m experimental flight station. Measured samples included $^{nat}$Mo [47], $^{95}$Mo, $^{96}$Mo, $^{98}$Mo, $^{100}$Mo [23], and two samples of $^{92/94}$Mo which provided a more accurate correction for the enhancement of the energy-averaged transmission. It also includes a differential scattering cross-section dataset for elemental Mo which was measured in the energy range between 0.5 and 20 MeV [48]. If high-resolution complimentary capture cross-section data were available, then a more complete analysis of the keV region for $^{95}$Mo would lead to a better overall data evaluation. In the unresolved resonance region, such complimentary capture cross-section data would better constrain the total cross-section SAMMY analysis. In the resolved resonance region above 2 keV, it would allow a more rigorous approach for parity and spin assignments based on $\gamma$-ray multiplicities. This is especially important since $^{95}$Mo has many low-lying states with different $J$ values [49]. Further evaluation of the measured isotopic Mo datasets could provide a statistical model calculation of $^{99}$Mo cross-section values as performed in Ref. [50].

Although the end products of this experiment and analysis are ENDF-compatible files, there are still several major problems that exist within the ENDF total cross-section representation. These issues have been identified by two major papers [10,32] and one international report by the Working Party on International Nuclear Data Evaluation Co-operation (WPEC) [52] and are described here for completeness. In ENDF format, the cross section in the URR is computed from average resonance parameters that are stored in ENDF file 2 and dilute cross sections stored in file 3 [15]. How these files are used is determined by an ENDF-102 LSSF flag [15]. When LSSF = 0, the dilute unresolved cross section is calculated from average parameters in file 2 and requires an additional partial background cross section from file 3 [15]. When LSSF = 1, the file 2 average resonance parameters contained in probability tables are converted to self-shielding factors and then multiplied by the cross section in file 3 with the same smoothness as the URR evaluation [14]. It is generally expected that the infinitely diluted cross section in file 3 should be obtained from the best combination of measurements and models as provided by evaluators [16]. The three papers propose the enforcement of the LSSF = 1 option and stress the importance of using resonance parameter interpolation instead of cross-section interpolation in the URR for more accuracy even though interpolating the cross section is a faster calculation. The FITACS analysis in the present paper ensures that the infinitely dilute cross sections calculated from the average resonance parameters in file 2 are in agreement with the cross section stored in file 3, which is not always the case. For example, the conversion of average parameters obtained from an optical model calculations into an equivalent single-level Breit-Wigner representation in ENDF can misrepresent the shape of the total cross section [52]. Another option that has been proposed for this region is to store unsmoothed high-resolution total cross-section experimental data directly [17,18] in evaluated files to be available to users who typically plot the infinitely dilute cross section versus energy without any self-shielding [14]. The ENDF format manual cautions that this should only be done if the structure represents a statistically significant number of levels (>10) to avoid "double shielding" [15]. Finally there is an ongoing effort to develop a generalized nuclear data format [53] as a modern alternative to replace the ENDF format, which was developed in the 1960s.

## ACKNOWLEDGMENTS

The authors would like to thank P. Brand, M. Gray, M. Strock, and A. Kerdoun for their efforts in operating the LINAC and their help in setting up experiments. They would also like to thank T. Sutton, P. Romano, C. Lubitz, B. Becker, P. Schillebeeckx, and T. Trumbull for helpful discussions regarding theory and analysis methods in the unresolved resonance region. This research endeavor was made possible with funding generously provided by Knolls Atomic Power Laboratory (KAPL).

[1] G. Leinweber, D. P. Barry, J. A. Burke, N. J. Drindak, Y. Danon, R. C. Block, N. C. Francis, and B. E. Moretti,Nucl. Sci. Eng. **164**, 287 (2010).
[2] J. Rest *et al.*, Argonne National Laboratory Report No. ANL-09/31, 2009 (unpublished).
[3] L. Mason *et al.*, National Aeronautics Space Administration Report No. NASA/TM-2011-217099, 2011 (unpublished).
[4] A. M. Phillips, G. S. Mickum, and D. E. Burkes, Idaho National Laboratory Report No. INL/EXT-10-19373, 2010 (unpublished).
[5] S. F. Mughabghab, *Atlas of Neutron Resonances: Resonance Parameters and Thermal Cross Sections Z* = 1–100 (Elsevier, Amsterdam, Netherlands, 2006).
[6] M. Chadwick *et al.*, Nucl. Data Sheets **112**, 2887 (2011).
[7] R. Bahran, Ph.D. thesis, Rensselaer Polytechnic Institute, 2013.
[8] N. Larson, Oak Ridge National Laboratory Report No. ORNL/TM-9179/R8, 2008 (unpublished).
[9] K. Shibata *et al.*, J. Korean Phys. Soc. **59**, 1046 (2011).
[10] J. Goorley *et al.*, Nucl. Technol. **180**, 298 (2012).
[11] P. K. Romano and B. Forget, Ann. Nucl. Energy **51**, 274 (2013).
[12] L. B. Levitt, Nucl. Sci. Eng. **49**, 450 (1972).
[13] R. E. MacFarlane and D. W. Muir, Los Alamos National Laboratory Report No. LA-12740-M, 1994 (unpublished).
[14] J. C. Sublet *et al.*, Commissariat á L'Énergie Atomique Report No. CEA-R-6227, 2009 (unpublished).

[15] M. Herman and A. Trkov, Brookhaven National Laboratory Report No. ENDF-102, 2009 (unpublished).
[16] D. E. Cullen, Lawrence Livermore National Laboratory Report No. LLNL-TR-461199, 2010 (unpublished).
[17] C. Lubitz (private communication).
[18] F. H. Fröhner and D. C. Larson, Nuclear Energy Agency Report No. NEA/WPEC-15, 1995 (unpublished).
[19] F. H. Fröhner, Nucl. Sci. Eng. **103**, 119 (1989).
[20] R. Bahran, M. Rapp, F. Saglime, D. Williams, Y. Danon, D. Barry, G. Leinweber, R. C. Block, and J. Hoole, *10th International Topical Meeting on Nuclear Applications of Accelerators (AccApp'11), Knoxville, 2011* (American Nuclear Society, Knoxville, TN, 2011).
[21] Y. Danon *et al.*, *Eighth International Topical Meeting Nuclear Applications and Utilization of Accelerators (AccApp'07), Pocatello, ID, 2007* (American Nuclear Society, Pocatello, ID, 2007).
[22] M. E. Overberg, B. E. Moretti, R. E. Slovacek, and R. C. Block, Nucl. Instrum. Methods Phys. Res., Sect. A **438**, 253 (1999).
[23] M. Rapp, D. Barry, R. Block, G. Leinweber, and Y. Danon, *American Nuclear Society Summer Meeting, Chicago, 2012* (American Nuclear Society, Chicago, 2012).
[24] P. Lambropoulos *et al.*, Nucl. Phys. A **201**, 1 (1973).
[25] M. Divadeenam, Ph.D. thesis, Duke University, 1968.
[26] M. V. Pasechnik, M. B. Fedorov, and V. D. Ovdienko, in All Union Conference on Neutron Physics, Kiev, 1980 (unpublished).
[27] F. Frohner, Nuclear Energy Agency Report No. OECD JEFF Report 18, 2000 (unpublished).
[28] F. Frohner, Gulf General Atomic Inc. Report No. GA-8380, 1968 (unpublished).
[29] H. Derrien *et al.*, Oak Ridge National Laboratory Report No. ORNL/TM-2000/129, 2000 (unpublished).
[30] P. Schillebeeckx *et al.*, Nucl. Data Sheets **113**, 3054 (2012).
[31] G. Noguere, Ph.D. thesis, Commissariat á L'Énergie Atomique, 2005.
[32] A. Carlson and H. Barschall, Phys. Rev. **158**, 1142 (1967).
[33] H. Feshbach, A. K. Kerman, and R. H. Lemmer, Ann. Phys. (N.Y.) **41**, 230 (1967).
[34] G. Pappalardo, Phys. Lett. **13**, 320 (1964).
[35] G. D. James, Nucl. Phys. A **170**, 309 (1971).
[36] I. Hall, Phys. Lett. **10**, 199 (1964).
[37] E. Rich, G. Noguere, C. De Saint Jean, and A. Tudora, Nucl. Sci. Eng. **162**, 76 (2009).
[38] F. H. Fröhner and O. Bouland, Nucl. Sci. Eng. **137**, 70 (2001).
[39] G. Audi, A. H. Wapstra, and C. Thibault, Nucl. Phys. A **729**, 337 (2003).
[40] K. S. Krane and D. Halliday, *Introductory Nuclear Physics* (Wiley, New York, 1987).
[41] P. Koehler (private communication).
[42] H. Utsumoniya *et al.*, Phys. Rev. C **88**, 015805 (2013).
[43] B. McDermott *et al.*, *American Nuclear Society 2013 Student Conference, Boston, 2013* (American Nuclear Society, Boston, 2013).
[44] S. C. van der Mark, Nucl. Data Sheets **113**, 2935 (2012).
[45] V. M. Shmakov *et al.*, Russian Federal Nuclear Center Report No. HEU-MET-FAST-092 NEA/NSC/DOC/(95)03/Volume II, 2012, https://www.oecd-nea.org/science/wpncs/icsbep/handbook.html.
[46] B. Richard, Ph.D. thesis, Centre CEA Valduc, 2012.
[47] (NEA-OECD, 2014), Vol. online database.
[48] M. Rapp, *et al.*, J. Korean Phys. Soc. **59**, 1745 (2011).
[49] F. J. Saglime, Ph.D. thesis, Rensselaer Polytechnic Institute, 2009.
[50] S. A. Sheets *et al.*, Phys. Rev. C **76**, 064317 (2007).
[51] A. R. De, L. Musgrove, B. J. Allen, J. W. Boldeman, and R. L. Macklin, Nucl. Phys. A **270**, 108 (1976).
[52] L. Leal and K. Shibata, Nuclear Energy Agency Report No. NEA/NSC/WPEC/DOC (2011) 430, 2011 (unpublished).
[53] C. M. Mattoon *et al.*, Nuclear Data Sheets **113**, 3145 (2012).